Citation (APA)
Esposito, R., Sasikumar, K., & Cabboi, A. (2026). Characterisation of reciprocating sliding friction for a cracked brick-mortar interface. *Materials and Structures/Materiaux et Constructions*, *59*(4), Article 201. https://doi.org/10.1617/s11527-026-03069-6

Materials and Structures (2026) 59:201
https://doi.org/10.1617/s11527-026-03069-6

ORIGINAL ARTICLE

Characterisation of reciprocating sliding friction for a cracked brick-mortar interface

Rita Esposito · Karthick Sasikumar ·
Alessandro Cabboi

Received: 30 August 2025 / Revised: 14 March 2026 / Accepted: 23 March 2026

Abstract The mechanical behaviour of masonry is strongly influenced by the brick-mortar interface. To isolate and benchmark the pure frictional response of this interface in mortared masonry, this study uses a reciprocating sliding tribometer test on cracked brick-mortar specimens. Tests were conducted under varying pre-compression levels and two reciprocating sliding frequencies, using unreinforced clay brick masonry with lime-cement mortar. Frictional behaviour was analysed through hysteresis curves relating the measured friction force to the sliding displacement. From these, the mean sliding friction coefficient and tangential stiffness were extracted for each cycle. Both parameters showed considerable variability across tests. The mean kinetic friction coefficients, typically ranging between 0.4 and 0.6, aligned with values from indirect tests methods (e.g., triplet or couplet shear tests), and their variability appeared independent of the applied normal load. In contrast, tangential stiffness showed a qualitative correlation with the normal load, despite a high scatter. To interpret the observed variability, statistical analyses including ANOVA and Principal Component Analysis were performed. Although further testing is required, these initial results offer valuable insights into the frictional mechanics of cracked masonry interfaces and suggest new testing avenues for more accurately characterising brick-mortar interaction in structural assessments.

Keywords Unreinforced masonry · Friction coefficient · Tangential stiffness · Energy dissipation · Tribometer

1 Introduction

The characterisation of the shear behaviour of unit-joint bonds is often performed with deformation-based tests in which both de-cohesion and friction mechanisms take place simultaneously [1–9]. Typical examples of tests are shear-compression tests on triplets [10] or couplets in the lab or shove tests on-site. For the interpretation of the experimental results, the assumption of the Amonton-Coulomb friction law is often made. Accordingly, the friction force is directly proportional to the normal load and governed by a coefficient of static or kinetic friction.

R. Esposito (✉)
Faculty of Civil Engineering and Geosciences, Department of Materials, Mechanics, Management & Design, TU Delft, Stevinweg 1, Delft 2628CN, The Netherlands
e-mail: R.Esposito@tudelft.nl

K. Sasikumar
Faculty of Civil Engineering and Geosciences, TU Delft, Stevinweg 1, Delft 2628CN, The Netherlands

A. Cabboi
Faculty of Civil Engineering and Geosciences, Department of Engineering Structures, TU Delft, Stevinweg 1, Delft 2628CN, The Netherlands
e-mail: A.Cabboi@tudelft.nl

Nevertheless, this assumption cannot be fully considered with the adopted testing methods, because both the de-cohesion and friction mechanisms are acting simultaneously.

Up to date, there are no dedicated tests to characterise the properties related to friction for mortared masonry. Such parameters, as friction coefficient and tangential stiffness, are especially relevant when considering the stability of arched structures (e.g., [11]), and the lateral resistance of in-plane and out-of-plane loaded walls (e.g., [12] [13]). Some information exists in the contest of mortarless or dry masonry (e.g., [14], this is numerical [15]), but this cannot be directly adopted to mortared masonry due to the different nature of the contact interface that exists between two masonry units, rather than involving failure at unit-joint bonds.

In pursuit of characterising the frictional response at the cracked brick-mortar interface in masonry, a reciprocating tribometer testing procedure is presented. This dynamic test provides information on the coefficient of friction, the tangential stiffness, and their variability, and on the energy dissipation associated to sliding friction. This study illustrates the methodology adopted to test the cracked brick-mortar interface and provides a preliminary investigation of influencing factors, such as pre-compression level, and reciprocating sliding frequency, for unreinforced clay brick masonry.

2 Materials and methods

2.1 Clay brick masonry

The tested material pairs are based on specimens extracted from unreinforced brick masonry, which were extensively characterised in previous experimental test series [16, 17]. Table 1 lists the main properties of the unreinforced brick masonry system. The latter was composed by solid clay brick masonry, which had nominal dimensions of 210 mm in length, 50 mm in height, 100 mm in thickness, and having a normalised compressive strength of 28.31 MPa. In addition, a pre-bagged mortar with the following characteristics was used: a 1:2:9 proportion in weight between cement, lime, and sand, a mean compressive strength of 3.81 MPa, and a mean flexural strength of 1.40 MPa.

Table 1 Properties of clay brick masonry adopted in this study according to [16, 17]

Property	Symbol	Unit	Average	CoV	No. of tests
Compressive strength	f_m	MPa	14.02	0.04	6
Elastic modulus	E	MPa	4640	0.25	6
Flexural bond strength	f_w	MPa	0.14	0.46	10
Initial shear strength	f_m	MPa	0.20		12
Friction coefficient	μ	-	0.69		12

2.2 Description of the tribometer setup

This study used the RTEC MFT-5000 reciprocating tribometer (Fig. 1). The test setup is constituted by two parts: a bottom moving plate that allows for a reciprocating motion, and a steady and horizontally leveled upper arm which holds a cylinder. The horizontal upper arm is connected through a hinge to the machine, to avoid bending moments at the location where the tangential force is measured. The normal force is imposed through an actuator, linked to the upper arm through a spring, and an automated control mechanism is in place to keep the normal force as steady as possible during the different runs. As a consequence, the upper part of the specimen is allowed to freely displace vertically, thus accomodating the dilatancy at the brick-mortar cracked interface. Normal and tangential forces are measured through piezo-force transducers, having a resolution of 15 mN and 4.5 mN, respectively. The bottom moving plate hosts a LVDT sensor for tracking the displacement, which has a resolution of 1 μm.

The allowable stroke for the reciprocating motion can be adjusted between 0.1 and 30 mm, and the reciprocating frequency can be varied between 0.1 and 80 Hz. The maximum frequency is chosen in order to stay well below the first resonance mode of the upper holding arm. To evaluate the response to friction in cracked masonry by tribometer tests, samples with a pre-existing crack at the brick-mortar interface (see the next section) were fabricated, and the specimen holder was modified (Fig. 1). A new upper cylinder casing was manufactured, with an external diameter of 19 mm and an internal diameter of 10 mm. The upper part of the specimen was held in

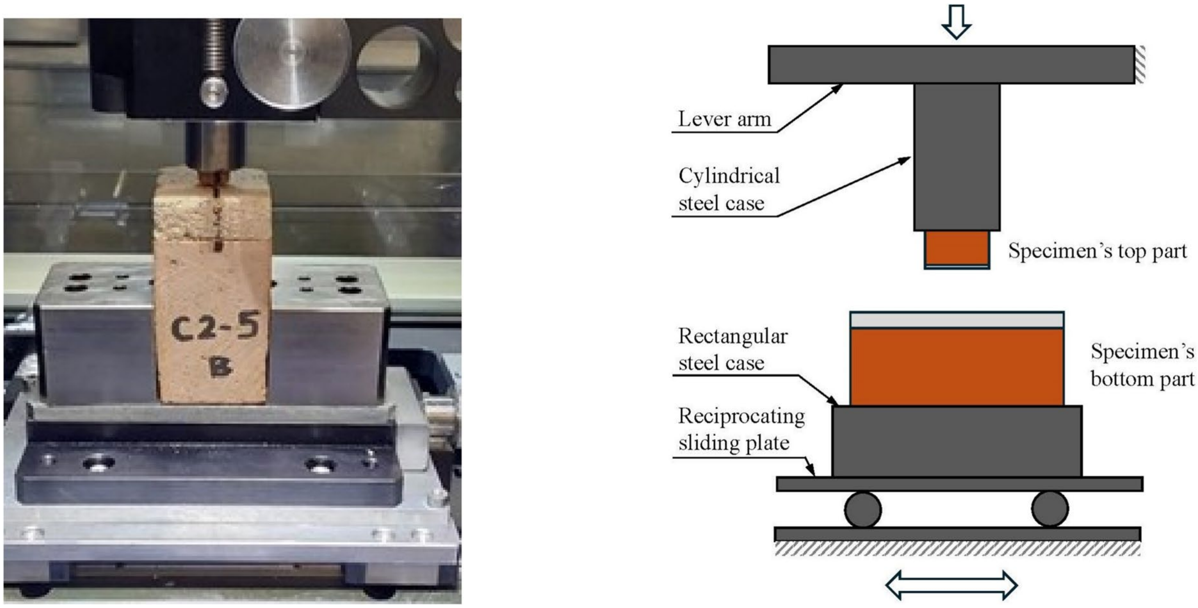

Fig. 1 Reciprocating tribometer setup and specimen with cracked brick-mortar interface

the metal casing for a depth of 45 mm that prevented its significant bending. The bottom part of the specimen, being a parallelepiped having cross-section of 30x30 mm, was mostly composed of the mortar joint and brick material. The portion of the brick was constrained in a metal casing connected to the bottom plate of the tribometer.

2.3 Specimen preparation

To manufacture specimens for the tribometer test, samples extracted from masonry couplets that had previously undergone a bond-wrench test were used. In this way, the cohesive bond at the brick-mortar interface was broken, resulting in the typical roughness of cracks in mortared masonry. Masonry couplets were built by a professional mason and hardened for various months in laboratory conditions. By using a computer-controlled bond wrench setup [18], each couplet was gradually cracked along the brick-mortar interface. Afterwards, the couplet was unloaded and the samples for the tribometer were extracted. The specimen for the tribometer test consists of a top cylindrical part made of brick and a lower parallelepiped part made of brick and mortar joint. To keep track of the location of both parts of the specimen during sawing, each couplet was divided into 8 areas having dimension 30x30 mm. Afterwards, the top part of the specimen was cored from the top brick and the bottom part was sawn. Both extraction procedures were performed with water. The top part of the specimen was glued into the metal case with heat melt adhesive glue, while the bottom part was mechanically clamped on the bottom plate.

2.4 Testing procedure

The tribometer enables reciprocating motion between the specimens in contact, while keeping a constant normal force level through an automated feedback controller and a fixed sliding distance. Each test was performed in two phases: first the required normal load was imposed and kept constant for 60 s, subsequently, the reciprocating sliding motion starts. Throughout the reciprocating motion and despite the controller, small variations of the normal forces still occur (see Section 3.2 for a more detailed discussion). The surface of each specimen was characterised by means of an optical profilometer scanning, using the VR-6200 Keyence profilometer with a measuring area of 1024×768 pixels and a resolution of 0.0074 mm. Surface texture properties are estimated according to ISO 4288:1996. However, only few surfaces were scanned again after the reciprocating sliding tests.

Two experimental series were performed (see Table 2): one series with a fixed reciprocating sliding frequency of 3 Hz, and a second series with a frequency of 0.2 Hz. Before the reciprocating sliding frequency takes over, the initial transition from static to kinetic friction (labeled as "first pull", which corresponds to the first quarter of the first cycle), is performed by imposing an initial pulling rate (see Section 4.1 for more details). The frequency value of 3 Hz was chosen based on shaking table test results of a full-scale building showing major sliding failure [19]. Whereas, a frequency of 0.2 Hz was chosen in the attempt to replicate quasi-static loading conditions that are used in standardised shear-compression tests for masonry. In both series of tests, the normal force was set up as a varying parameter, in order to check eventual variations of the coefficient of friction with an increasing pre-compression level. All tests have been performed considering a sliding distance of ±0.4 mm. This resulted in a total stroke of 0.8 mm. The reason behind this choice was to look for a sliding distance that would be large enough to extract a coefficient of friction for sliding, but short enough to avoid the sliding over a completely new contact area. For each test, a total number of 180 cycles fixed. At least 3 material pairs for each normal force were tested. It should be noted that the pre-compression stress levels reported are to be considered as nominal values, since the real area of contact is not known at every instant during the test. Hence, the applied nominal contact pressure, see Table 2, refers to the geometrical cross-section in contact of the top part of the specimen.

Table 2 Loading parameters considered in the different test series

Specimen name	Normal force (N)	Nominal contact pressure (MPa)	Freq. (Hz)
C1-12-6-A	6.4	0.10	0.2
C2-1-6-A	6.4	0.10	0.2
C2-4-6-A	6.4	0.10	0.2
C1-7-13-A	12.8	0.20	0.2
C3-9-13-A	12.8	0.20	0.2
C1-10-25-A	25.5	0.40	0.2
C2-8-25-A	25.5	0.40	0.2
C3-10-25-A	25.5	0.40	0.2
C1-3-38-A	38.2	0.60	0.2
C2-3-38-A	38.2	0.60	0.2
C3-3-38-A	38.2	0.60	0.2
C3-11-8-B	8	0.13	3
C1-8-13-B	12.75	0.20	3
C2-2-15-B	15.39	0.24	3
C3-8-20-B	20.2	0.32	3
C1-5-29-B	28.35	0.45	3
C1-4-34-B	34.1	0.54	3
C2-7-34-B	34.1	0.54	3
C3-6-34-B	34.1	0.54	3

3 General observation on the experimental results

3.1 Surface characterisation

For each specimen, the two surfaces in contact were characterised by means of a profilometer before the test; this provides an indication of the surface roughness (Fig. 2). The following parameters were measured for each surface in contact of each specimen: the mean peak height S_a, the sum of the largest peak height value and the largest pit depth S_z, the mean peak curvature S_{pc}, and the surface texture aspect ratio S_{tr}. An overview for all specimens is given in Table 3.

On average the two surfaces, belonging to the bottom and top portion of the specimens, present similar features being very rough and uneven. The mean peak height S_a is close to 200 μm for both surfaces, indicating a high roughness since $S_a > 20$ μm. Values of S_z larger than 0.1 mm indicate the presence of an uneven surface. The mean peak curvature values S_{pc}, also indicate that the peaks on the surfaces are rather sharp, since $S_{pc} > 0.01$ mm^{-1}. The values of the surface texture aspect ratio S_{tr} are rather low, hence, the bottom surface texture can be characterised as anisotropic ($S_{tr} < 0.5$ indicates a strong isotropy, while $S_{tr} < 0.3$ is strongly anisotropic). This texture anisotropy could be expected, since the mortar is applied on the brick in a preferential direction during the construction of the specimen. Overall, a high value of surface roughness and uneven surfaces with sharp peaks may be prone to wear. Therefore, during the sliding process between the two surfaces, debris can be generated and "rolled over", into cylindrical, spherical, and needle-shaped particles [20]. The wear

Table 3 Surface properties measured before carrying out the reciprocating sliding tests. Parameters S_a, S_z, S_{pc} and S_{tr} correspond to the mean peak height, sum of the largest peak height value and the largest pit depth, the mean peak curvature, and the surface texture aspect ratio, respectively

Surface property	Bottom specimen surface				Top specimen surface			
	mean	std. dev.	min	max	mean	std. dev.	min	max
S_a (μm)	215	78	127	501	189	74	23	395
S_z (mm)	3.3	1.6	1.4	5.6	1.5	0.6	0.8	2.7
S_{pc} (1/mm)	6.5	0.6	5.6	8.0	11.5	6.2	5.0	36.7
S_{tr}	0.35	0.13	0.14	0.62				

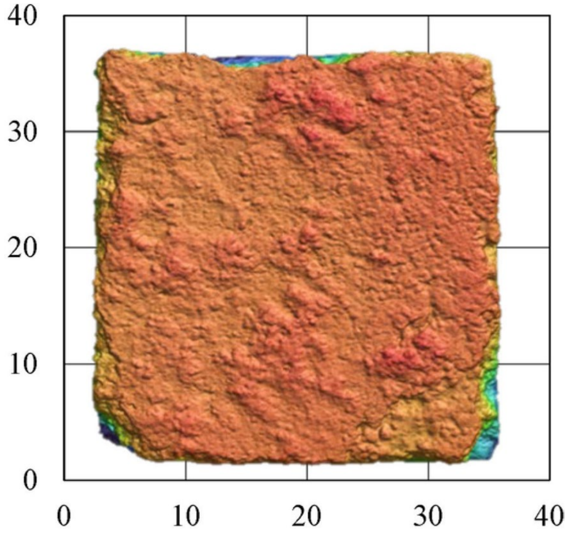

Fig. 2 Example of a profile scan of the bottom part of the specimen before running the reciprocating sliding tests

debris can also stay trapped between the surfaces, which is often called the "third body", and can form a heterogeneous interfacial layer that can drastically affect the friction and wear behaviour [21].

3.2 Interpretation of recorded hysteresis cycles

Figures 3a,b show two examples of measured hysteresis cycles at two different normal forces and reciprocating frequencies, depicting the evolution of the coefficient of friction with reference to the sliding distance. The friction coefficient is calculated by dividing the measured friction force by the measured normal force. In both graphs, the black line indicates the first pull, while the blue lines refer to the subsequent reciprocating motion cycles. Note that the non-zero value of the starting point of the first pull is simply due to an original offset in the LVDT readings, after normal contact is established between the two surfaces of the specimen. In general, once the reciprocating motion starts, the coefficient of sliding friction tends to "settle" at higher values than those observed during the first pull. This was observed for all tests, except for those performed with low normal forces (3.2 and 6.4 N) and one test carried out at 38.2 N (C3-3).

Despite the repeatable shape of the hysteresis loops, the coefficient of friction varies during each cycle. This variation is already rather pronounced during the first pull. Considering the nature of the contact surfaces, which are rather rough, uneven and characterised by sharp peaks, these variations in the friction coefficient may be due to the evolution of wear and the resulting debris interposing between the contact surfaces, as also discussed in [22] for reciprocating sliding tests carried out between two steel specimens. Wear debris also accumulate on the sides of the contact area, as shown in Fig. 4b, which may cause a contact misalignment during the reciprocating sliding motion. The latter can result into an asymmetric behaviour for sliding friction, along the left or right direction, and to a variation of the normal force (as also shown in Fig. 4a). For this reason, the kinetic coefficient of friction has been computed for sliding distances between −0.1 and +0.1 mm around the origin, where the normal force remained nearly constant (see Fig. 4a). As a general note, the normal force variation throughout all the tests tends to be around 1-2% with respect to the pre-imposed value. However, a small variation of the normal force, if caused by vertical contact misalignment throughout the sliding process, can lead to larger variations of the friction force, as explained in [23–25]. Such variation of the friction

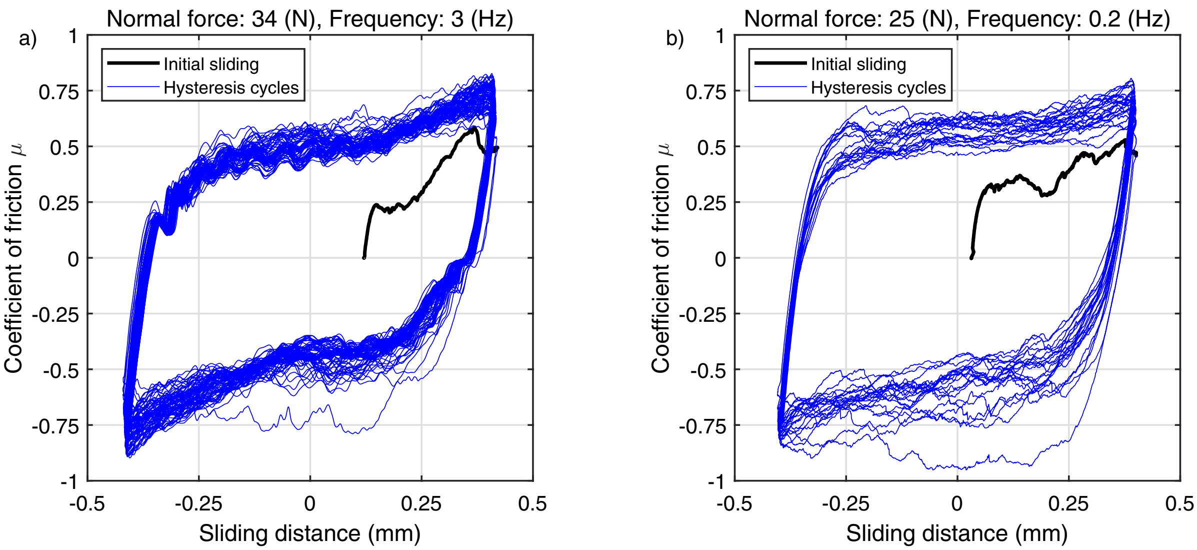

Fig. 3 Examples of measured hysteresis cycles: **a** Normal force at 34 (N) and reciprocating frequency at 3 (Hz) (Couplet C1-4); **b** Normal force at 25 (N) and reciprocating frequency at 0.2 (Hz) (Couplet C1-10)

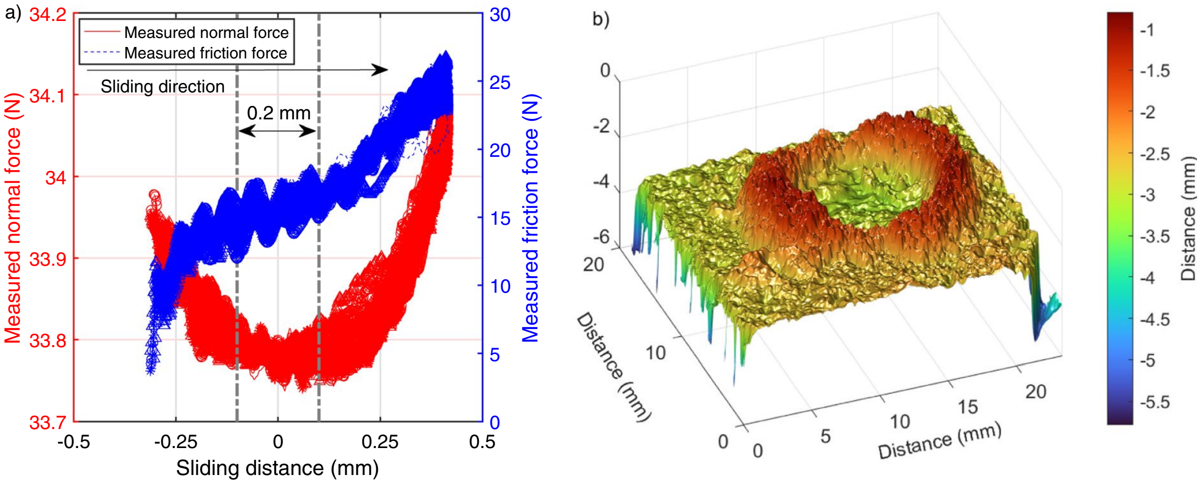

Fig. 4 **(a)** Estimation of the kinetic coefficient of friction in a region with nearly constant measured normal force (Couplet C1-4); (**b**) accumulation of debris observed from profilometer measurement after the tribometer test

force is also visible in Fig. 4a, which is not linearly proportional to the variation of the normal force during sliding. Section 4.2 provides a more in-depth discussion with reference to the identification of kinetic friction.

Between the first and last cycle, the hysteresis curves show a relevant variation in energy dissipation and a potential influence of normal force and/or sliding frequency on the hysteresis behaviour. To estimate the dissipated energy, the energy ratio established in [26] and discussed in [27] is used:

$$A = \frac{E_d}{E_t} = \frac{E_d}{4d\mu N} \tag{1}$$

where A is called the energy ratio for each cycle, E_d is the energy per cycle measured by estimating the enclosed area by a hysteresis loop, and E_t is the energy that would be dissipated if sliding would be characterised by an ideal Coulomb-like behaviour; d is half of the total sliding distance from left to right. The variation of the dissipated energy is discussed further in Sect. 4.3.

At last, in all hysteresis cycles, a slope is visible at the reversals of motion, indicating the presence of a tangential stiffness during the static-kinetic transition phase. Figure 5 shows how the tangential stiffness is calculated for all cycles. The slope of the friction force vs displacement curve around the crossing through zero of the friction force is considered. In each cycle, two values are calculated, one on the right and on the left side of the curve; additionally, the average of the two values is also considered. A more detailed discussion on this aspect is provided in Sect. 4.4.

4 Analysis of the experiments

4.1 Transition from static to kinetic friction

Figure 6 displays how the coefficient of friction varies along the initial sliding distance that occurs during the start of the reciprocating motion. This first pull defines the first transition from rest to gross sliding. The choice of using the coefficient of friction rather than the measured friction force enables a comparison among the different curves measured at different normal forces. For the test carried out at a reciprocating sliding frequency of 3 Hz, three different ranges of normal forces were used: 5–15 N, 15–25 N and 25–35 N (see Fig. 6a). For the test conducted at a reciprocating sliding frequency of 0.2 Hz, four specific values of normal forces were used (see Fig. 6b). In general, during the first pull, a build-up of the friction force can be observed, which is linked to the presence of a tangential stiffness, until a maximum (static friction) is reached, after which sliding occurs. However, both sets of tests, independently of the sliding frequency, show a large variability and a lack of repeatability of the results of the coefficient of friction during the first pull. In addition, the transition from static to kinetic friction is not always obvious. Note that this variability is not related to the variation of the normal force, which is relatively constant compared to the variation of the friction force (see Fig. 4a). The influence of the normal force on the estimated coefficient of friction, can only be observed for a selected number of curves, shown in Fig. 7, in which the experiments carried out at a normal force below 20 N were excluded. By clustering all the remaining curves into two ranges, 20-30 N and 30-40 N, it can be observed that the tests performed at a lower normal force tend to exhibit a slightly faster build-up of the friction force (higher initial coefficients of friction), while the build-up of the friction for the tests performed at a higher normal force is somewhat slower. Interestingly, such an initial effect of the normal force completely disappears once gross

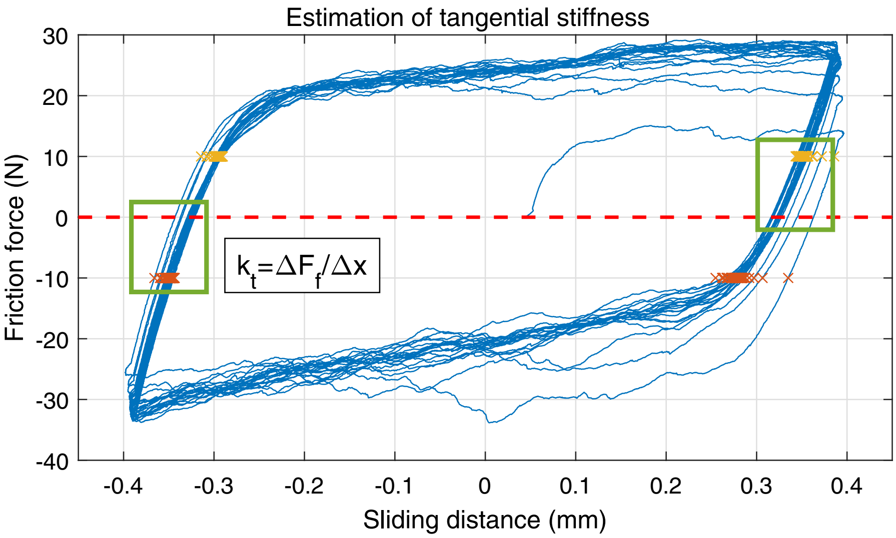

Fig. 5 Estimation scheme for the tangential stiffness, k_t. The green boxes indicate the region of data used to compute the tangential stiffness, for the right and left side of the hysteresis curve. The curve refers to couplet C1–3, measured at 0.2 Hz and for a normal force of 38.2 N

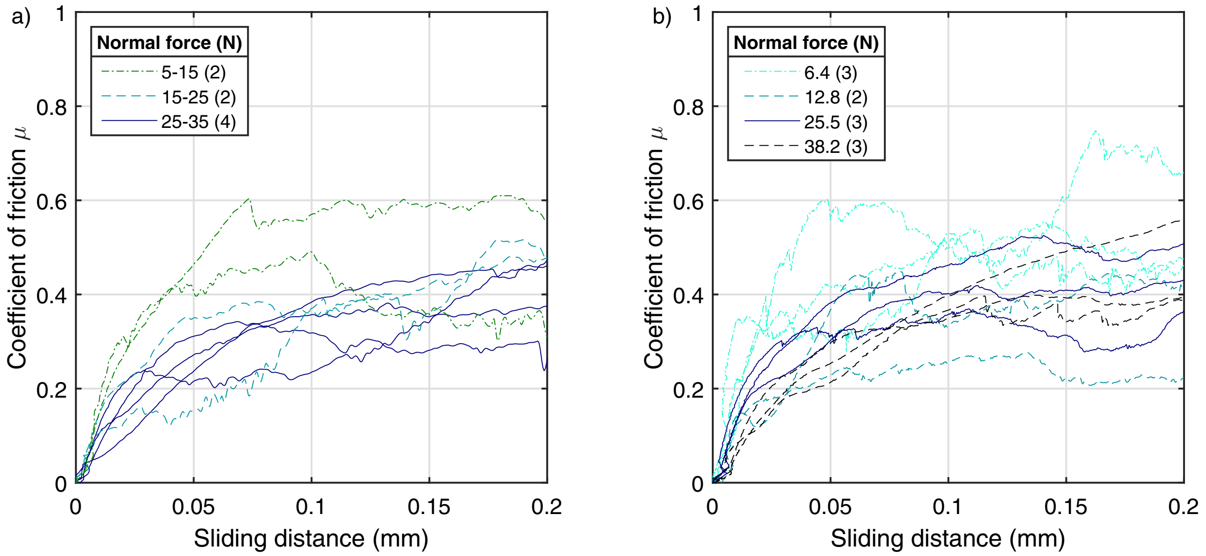

Fig. 6 Initial part of the hysteresis cycles: transition from the static to the kinetic friction regime. Test carried out at (**a**) 3 Hz and (**b**) 0.2 Hz. The legend indicates the normal force values and ranges and the number of tests in brackets. The averaged speed of the moving plate, from 0 to 0.2 mm is 0.71 mm/s and 0.17 mm/s, respectively

sliding starts, probably masked by the variability of the friction force during sliding, caused by the evolution of the wear debris. A possible source of variability between the two sets of tests could be that the rate at which the bottom plate moves, (i.e. the rate of the applied pulling force to the upper specimen), is not constant during the first pull. An average speed of 0.71 mm/s and 0.17 mm/s, for the test at 3 Hz and 0.2 Hz, respectively, was computed for the displayed sliding distance.

In general, a possible explanation of the high variability could be due to the influence of roughness, contact misalignment and the creation of wear debris caused during the first pull. The effect of contact misalignment was briefly mentioned in Sect. 3.2, whereas the influence of roughness for the test case at hand can be difficult to quantify, since the initial high roughness of the surfaces in contact (see surface profile parameters in Table 3), characterised by high asperities peaks (e.g. high values of S_z), tend to evolve rather quickly due to wear, which is pronounced by the brittleness nature of the surface itself. An attempt was made to find a possible correlation between the measured surface profile properties (indicated in Table 3) and the static-kinetic transition curves shown in Fig. 6. Besides the following observations, no explicit correlation was found. With reference to Fig. 6a, the highest two curves (see the two dotted green lines reaching values of μ between 0.5−0.6 around a displacement of 0.07 mm) correspond to two material pairs, for which the S_Z of the mortar surface reached the highest values, around 5.5−5.6 mm, well above the mean and exceeding the variation of the standard deviation. The static-kinetic transition curve with the lowest value of friction (see dashed line that has a value of μ below 0.2, around a displacement of 0.05 mm), corresponds to a material pair which has the S_a and S_z of the mortar surface at 157 μm and at 1.7 mm, respectively. Both well below the mean values and near the minimum.

In an attempt to look for possible correlations between the behaviour of the friction force during the initial pull and the surface parameters, Fig. 8 shows the relation between the estimated area under the curves shown in Fig. 6, for a sliding distance of 0.05 mm and the S_z parameter of the top specimen. In general, it seems that such area tends to decrease for increasing values of S_z, suggesting that the presence of a more pronounced difference between the largest pit depth and peak height of the top specimen decreases the coefficient of friction. This seems to be observable for both set of tests (Fig. 8a-b).

As mentioned before, the influence of roughness and wear on the reported results are rather

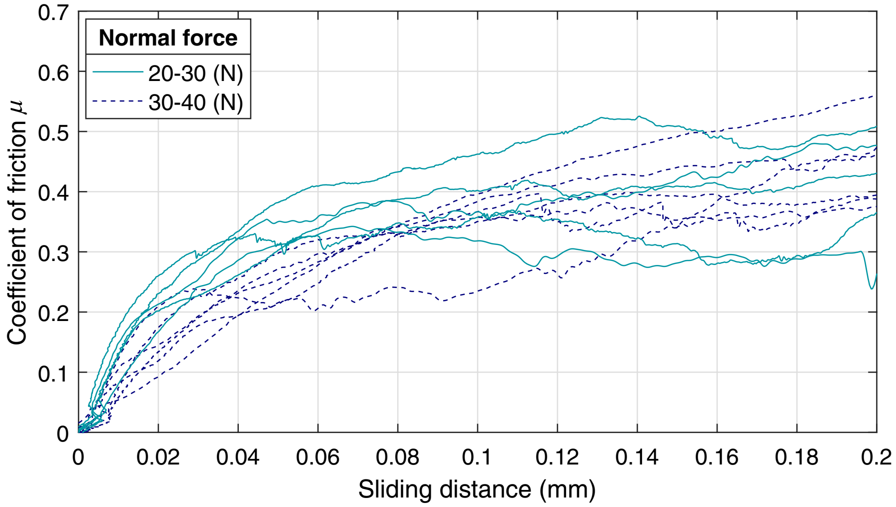

Fig. 7 Initial part of the hysteresis cycles: transition from the static to the kinetic friction regime. The curves are clustered according to two normal force ranges, independently of the reciprocating sliding frequency

challenging to quantify from this preliminary study, and the results reported in the literature are also somewhat controversial. For instance, if the wear debris exhibit a cylindrical shape, they could act as small roller bearings, inducing a lubricant-like effect, reducing sliding friction, as shown in [28]. In the latter study, reciprocating linear sliding experiments were carried out, between a silicon ball on a silicon flat specimen, and a "third-body" layer was formed, generating roll-like debris during the sliding process. Due to the "rolling effect", the coefficient of sliding friction decreased from 0.6 to 0.2, approximately. The same phenomenon was observed in [29, 30] for different material pairs. Similar conclusions were also drawn in [31], even though the research refers to a completely different field, such as geomechanics. The study shows that the sliding and corresponding wear process, during shear tests for rocks, led to small and cylindrical rolls made of nanoparticulate gouge. This caused a drastic friction force weakening, due to a rolling-dominated sliding process, in which friction sliding coefficients generally dropped, also up to 50% of its initial peak value, before the formation of such roller-like debris. Further results in which the friction

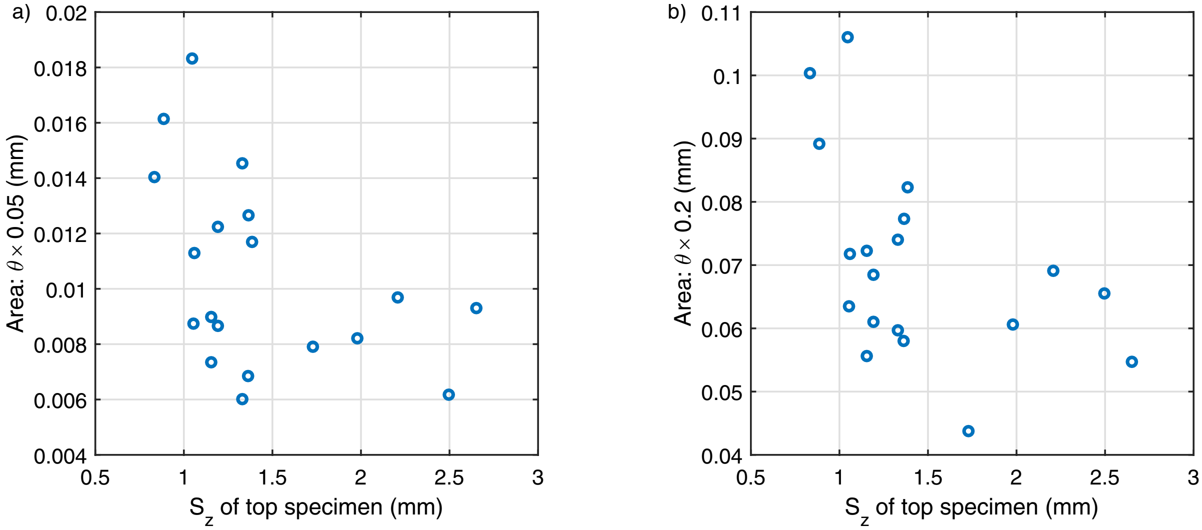

Fig. 8 Correlation graphs of ($\mu \times$ d) vs. S_z, where d is the sliding distance selected at 0.05 mm (**a**) and 0.2 mm (**b**) The estimated area refers to the curves shown in Fig. 6. No classification between reciprocating frequencies is made

coefficient reduces due to wear debris can be found in [32], which discusses the tendency of the wear debris to form a protective tribolayer.

However, if the particles forming the wear debris do not act as a roller, an increase in the friction coefficient can be observed, due to an increase in the plowing effect, as shown in [33]. The plowing effect due to wear debris can also be simulated through a model developed in [34], which showed a qualitative good agreement with experimental results discussed in a companion paper, see [35], and later on in [36]. In [37], severe wear rate also led to an increase of the friction coefficient.

For the case at hand, it is hard to guess whether the wear debris induces a lubricant-like effect or whether the plowing effect is more dominant. It could well be that both mechanisms are at play, and the interaction between them generates the observed scatteredness of the data. It is important to note that, generally, friction estimates are performed after reaching a steady-state phase of the friction force. In fact, fretting experiments can be divided in three phases: running-in phase, steady-state-wear phase and wear-out phase [38]. The tests in this study refer to the running-in phase, which may also explain the large variability.

4.2 Sliding friction

Based on the procedure outlined in Sect. 3.2, the sliding coefficient of friction was estimated for a segment of data in which the normal force and the friction force exhibited the lowest variation, indicating a horizontal trajectory (parallel to the sliding direction) of the measured friction force. A more detailed explanation concerning the effect of an inclined measured friction force can be found in [23, 24], and specifically for the adopted testing device, the readers can refer to [25]. Figures 9a-b, refer to the estimated friction coefficients for the tests carried out at 3 Hz, with reference to the sliding along the right and left direction, respectively. The same holds for Figs. 10a-b, but with reference to the tests carried out at 0.2 Hz. For these figures, the results are presented in terms of boxplots, for which the central line indicates the median, the boxes define the interquartile range (IQR), the whiskers capture the extension to 1.5×IQR, and the red markers define the outliers. The results are also clustered based on different normal force ranges, as already shown in Fig. 6. On one hand, for both sets of tests (at 3 Hz and 0.2 Hz), a large variability is observed and no clear dependence between the kinetic coefficient of friction and the normal force can be noted. On the other hand, on average, the median values for the tests performed at 0.2 Hz (ranging between 0.4 and 0.63) seem all slightly higher than the median values obtained for the tests carried out at 3 Hz (medians of μ between 0.4−0.5). This general increase seems to apply to both directions.

Roughly speaking, the kinetic friction coefficients seem to vary between 0.4 and 0.6. These values are in line with other values identified from different experimental studies on clay brick masonry as reported for example in [5], [39], [40].

4.3 Dissipated energy analysis

The cyclic tests enables an estimation of the dissipated energy per cycle. Figure 11a displays the evolution of the averaged normalised area estimated for every cycle and for all the tests done at 0.2 Hz (cyan solid line) and at 3 Hz (blue solid line). The energy per cycle is normalised by simply dividing each area by the maximum area identified through a single test. Averaging of these normalised area for each test is performed by looping through each cycle. Note that tests carried out at 0.2 Hz contain less cycles, since each cycle lasts longer. Both curves show a similar trend: the normalised energy per cycle tends to decrease for the first 50 cycle. After the first 50 cycles, the tests carried out at 3 Hz exhibit a roughly horizontal trend, with a slight increase in the normalised energy. This trend is mirrored by the trend of the averaged values of the sliding coefficient of friction, obtained for every cycle and averaged through the different material pairs. Figure 11b shows the distribution of the energy ratio obtained by applying Eq. (1). All energy ratios are reported for each cycle and for each test. Energy ratios less than 1, indicate that the area of a measured cycle is smaller than the energy related to an ideal cycle governed by Coulomb friction damping. This is mainly due to the contribution of the tangential stiffness, which regularises the hysteresis behaviour whenever a velocity reversal occurs. However, values greater than 1 are also observed, and this could be linked to the presence of sharp and high peaks in the hysteresis curves, and due to differences

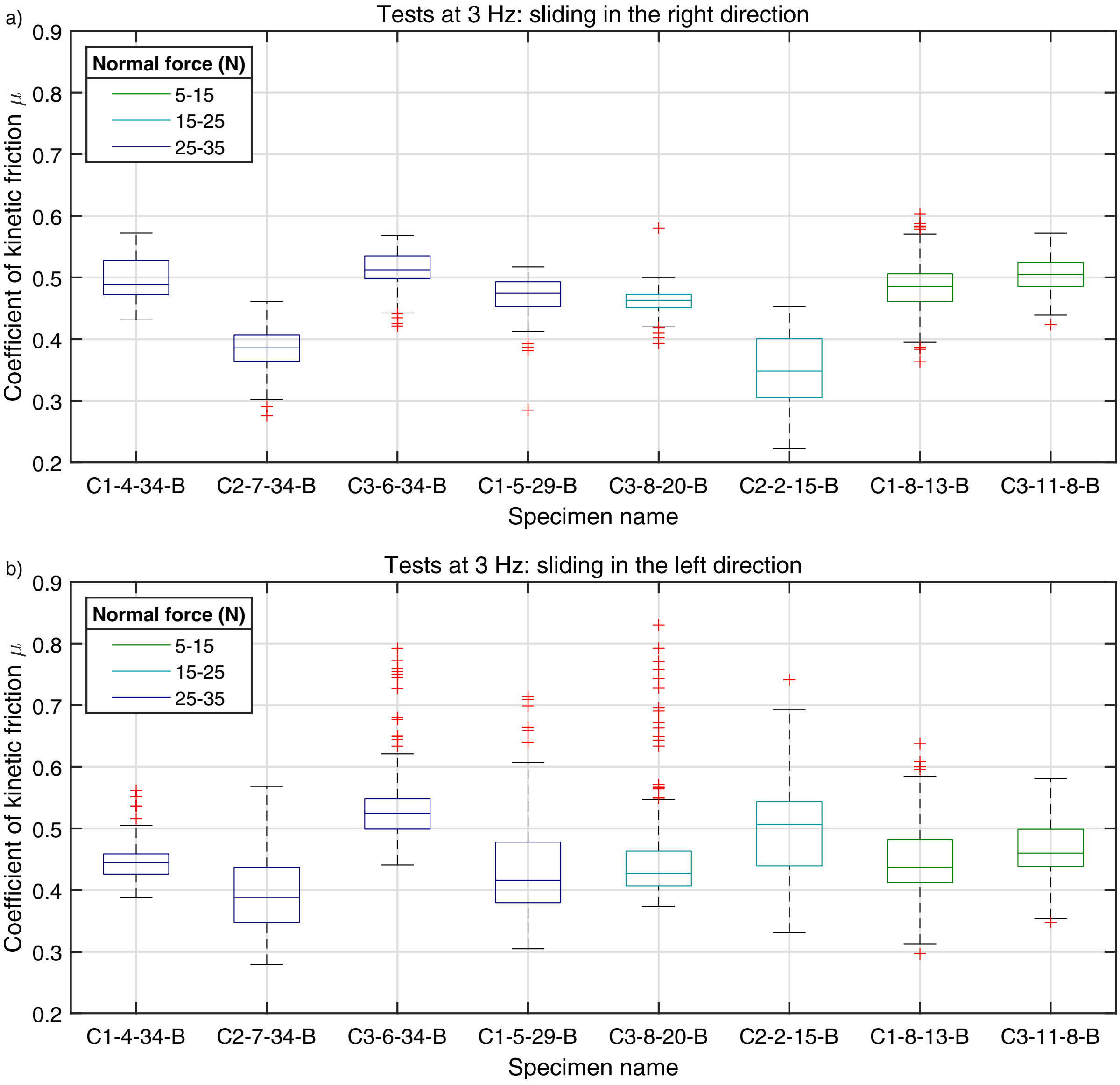

Fig. 9 Boxplot of estimated kinetic friction coefficients for different material pairs, tested at a reciprocating sliding frequency of 3 Hz and under different normal forces. The median is indicated by the central line, with boxes representing the interquartile range (IQR). Whiskers extend to 1.5×IQR, while red markers denote outliers. Figure (**a**) refers to the values estimated for the sliding to the right, while figure (**b**) refer to the sliding to the left

of the friction coefficient estimated near the equilibrium position of the slider (−0.1 mm to +0.1 mm) and towards the edge of the hysteresis curves (sometimes slightly higher than the identified kinetic friction values). Examples of such curves are provided in Fig. 12. Overall, the dissipated energy analysis seems to indicate an initial tendency to dissipate more energy during the first cycles (due to initial wear). In addition, the contribution of the tangential stiffness seems rather relevant, since it causes deviation from an ideal Coulomb-driven system.

4.4 Tangential stiffness

The reference to tangential stiffness, rather than to a tangential contact/interface stiffness (k_i), is a

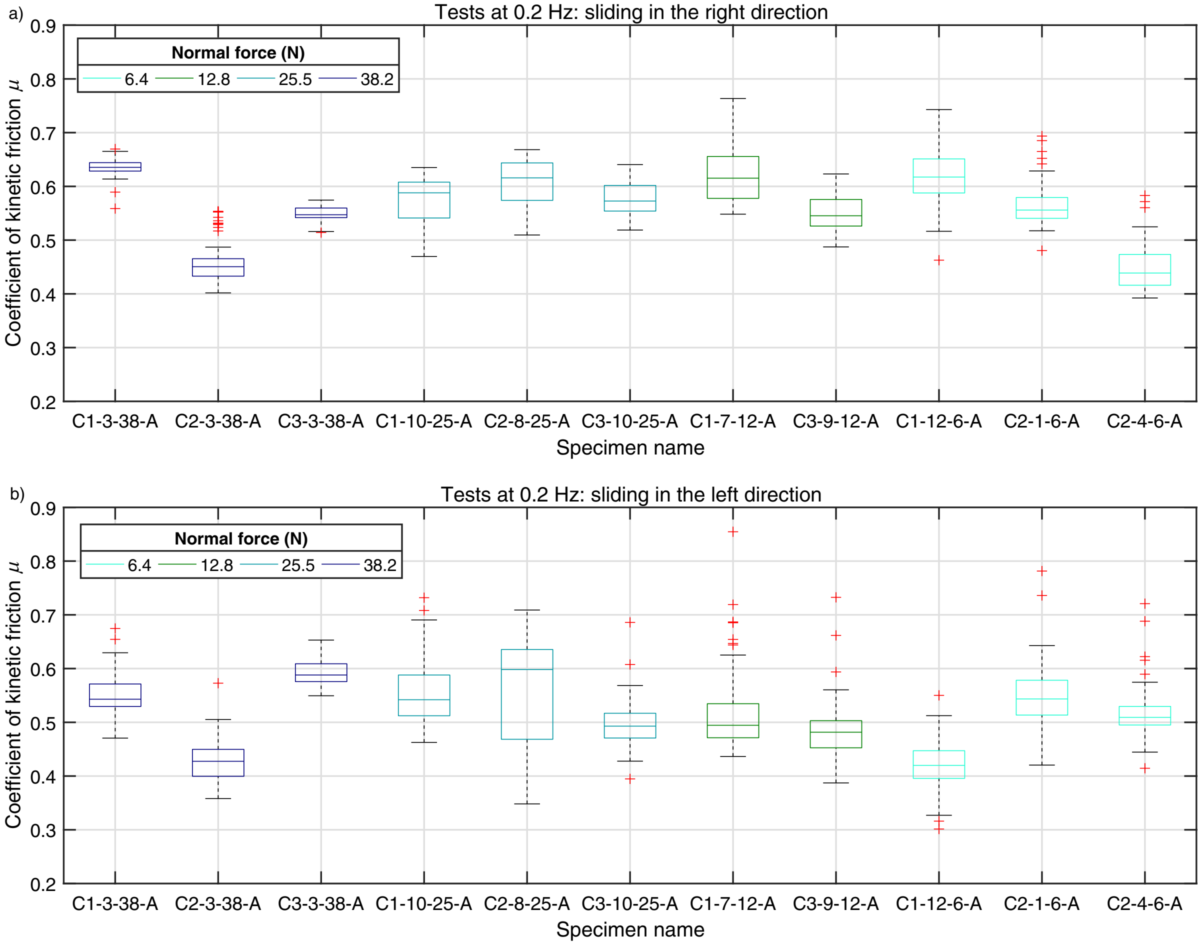

Fig. 10 Boxplot of estimated kinetic friction coefficients for different material pairs, tested at a reciprocating sliding frequency of 0.2 Hz and under different normal forces. The median is indicated by the central line, with boxes representing the interquartile range (IQR). Whiskers extend to 1.5×IQR, while red markers denote outliers. Figure (**a**) refers to the values estimated for the sliding to the right, while figure (**b**) refers to the sliding to the left

deliberate choice, since the distinction between the bulk stiffness (k_b) of the specimen in the tangential direction, the stiffness of the holding system (k_{hold}) and the interface stiffness itself was not possible. Note that during the velocity reversal phase, the piezo-force transducer, that is supposed to measure the tangential force (which is equivalent to the friction force, whenever inertial forces of the upper arm can be neglected), will detect a displacement dependent force that governs the transition from a partial-slip phase to the sliding phase. In principle, this transition is governed by the tangential contact stiffness, as discussed in [41]. However, since the contribution of the specimen's stiffness is unknown, the measured force during partial slip is proportional to an equivalent stiffness, which reads as follows

$$\frac{1}{k_{eq}} = \frac{1}{k_i} + \frac{1}{k_b} + \frac{1}{k_{hold}} \tag{2}$$

in which k_{eq} corresponds to the estimated stiffness from the reciprocating sliding measurement during the partial slip (or velocity reversal) phase. The estimation was performed for the left and right partial slip phase, hence, twice per cycle. Figures 13a,b display boxplots for each material pair, and for the tests carried out at 0.2 and 3 Hz, respectively. A boxplot, for each material pair, represents the main statistical

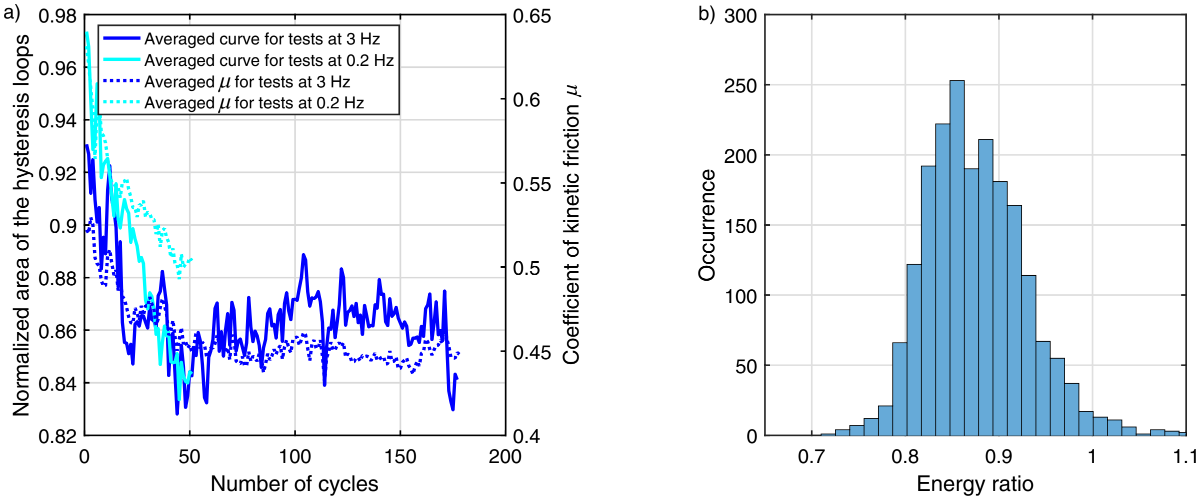

Fig. 11 **a** Averaged curves for the normalised area of the hysteresis loops, for tests carried out at 3 and 0.2 Hz; **b** distribution diagram of the energy ratio, representative of all the tests

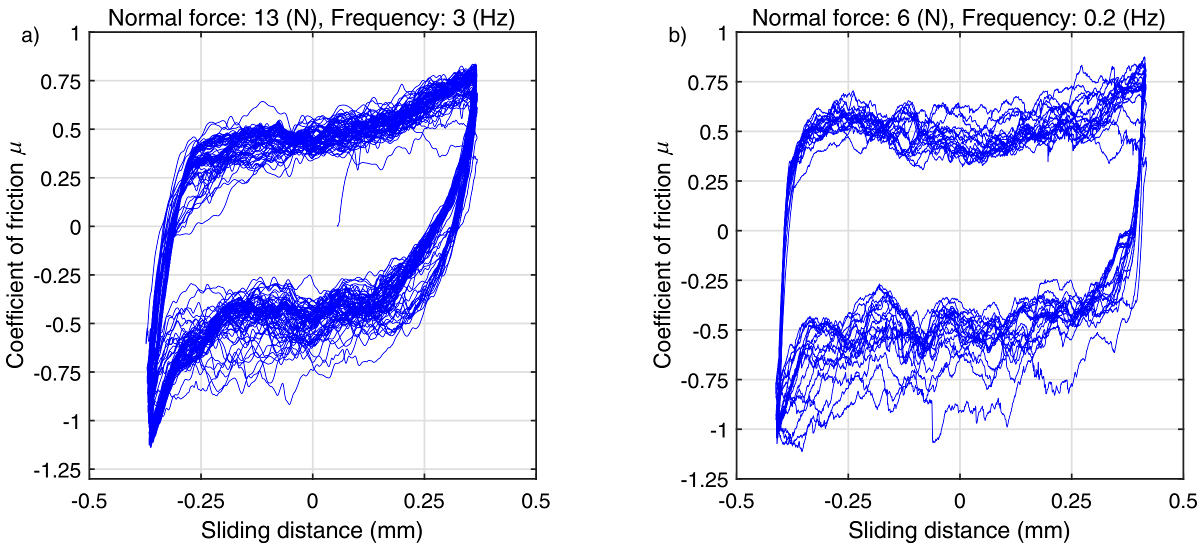

Fig. 12 Examples of measured hysteresis cycles exhibiting a lack of symmetry between the two sliding direction: (**a**) Normal force at 12.75 (N) and reciprocating frequency at 3 (Hz) (Couplet C1-8); (**b**) Normal force at 6.4 (N) and reciprocating frequency at 0.2 (Hz) (Couplet C2-4)

information of all the estimated values of the tangential stiffness during that specific test. In general, for both data sets, the median values roughly range between 100 and 400 N/mm. Most of the material pair exhibit a rather large scatter of the estimated values, with few exceptions (see C3-3-38-A and C1-5-29-B). For both figures, the largest scatter can be observed for the tests carried out at a low normal force, which also exhibit the lowest values of the tangential stiffness. In contrast to the observations made for the estimated sliding friction coefficients, the tangential stiffness seems to somehow depend on the normal force in a rather qualitative way. To emphasise this, the estimated values of the tangential stiffness were averaged

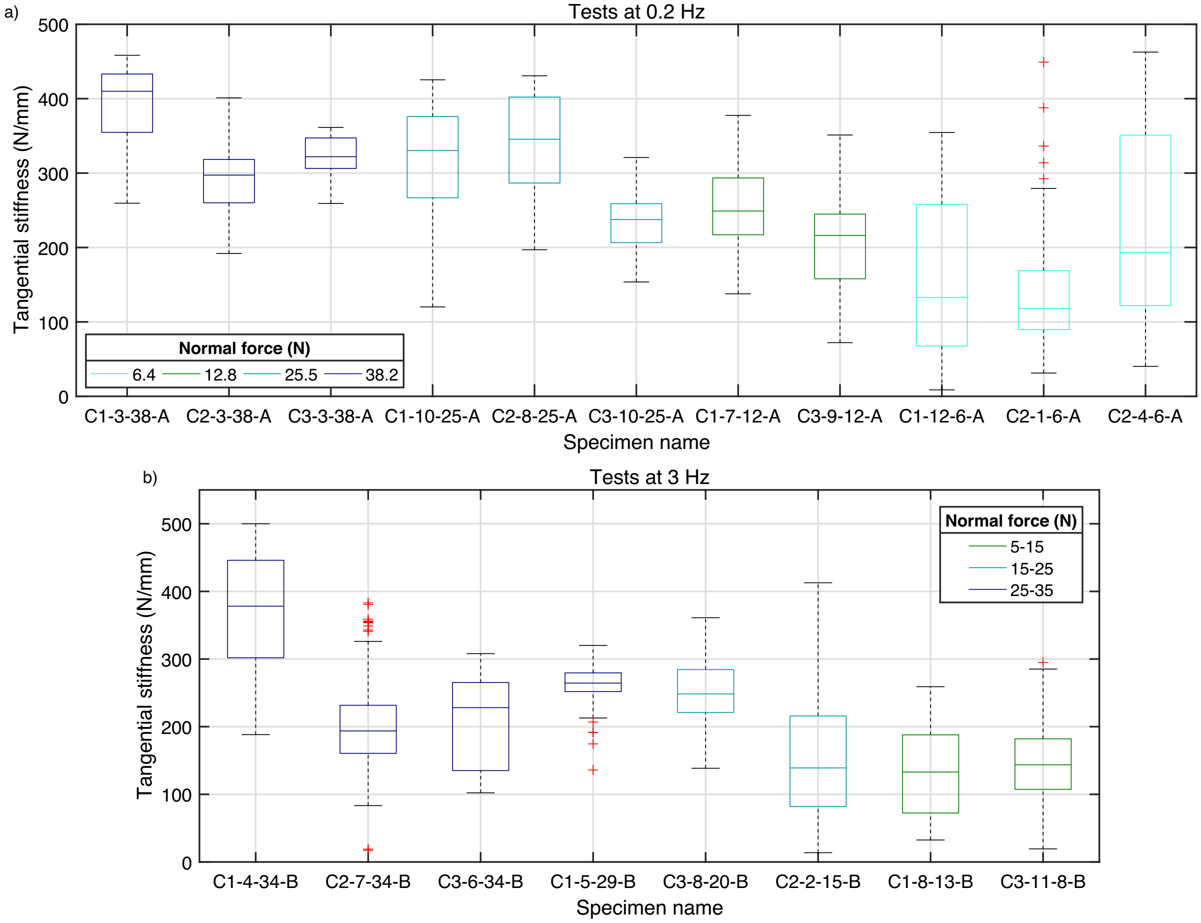

Fig. 13 Boxplot of estimated tangential stiffness for different material pairs, tested under different normal forces. The median is indicated by the central line, with boxes representing the interquartile range (IQR). Whiskers extend to 1.5×IQR, while red markers denote outliers. Figure (**a**) refers to the values estimated for tests carried out at 0.2 Hz, while figure (**b**) refers to the tests conducted at 3 Hz

for each material pair throughout the number of cycles. For each material pair, two averages were provided: one refers to the values estimated to the right, and one to the left side of the hysteresis curves. The choice of this separation is due to the fact that a non-negligible difference between the stiffness of the two sides was observed. The averaged results are then displayed with reference to the change of the normal load, as shown in Figs. 14a,b, which refer to the test carried out at 0.2 and 3 Hz, respectively. For all data sets, the blue dots, which correspond to the averaged tangential stiffness of the right tend to be smaller than the values estimated on the left side (green dots). The red line defines the total average of all the estimated tangential stiffness values for a specific normal load.

For the tests carried out at 0.2 Hz, an increase of the tangential stiffness with increasing values of the normal force is observed. A similar trend can also be observed in Fig. 14b. Qualitatively speaking, the estimated stiffness values for the tests carried out at 3 Hz seem to exhibit lower values than the ones estimated for the tests at 0.2 Hz. The tangential stiffness is a relevant parameters in numerical modeling of masonry, but it is rarely experimentally determined in the case of mortared masonry. In particular, it is relevant for the class of simplified block-based models in which mortar joints and brick-mortar bonds are lumped in a single interface element (e.g. [42], [43]).

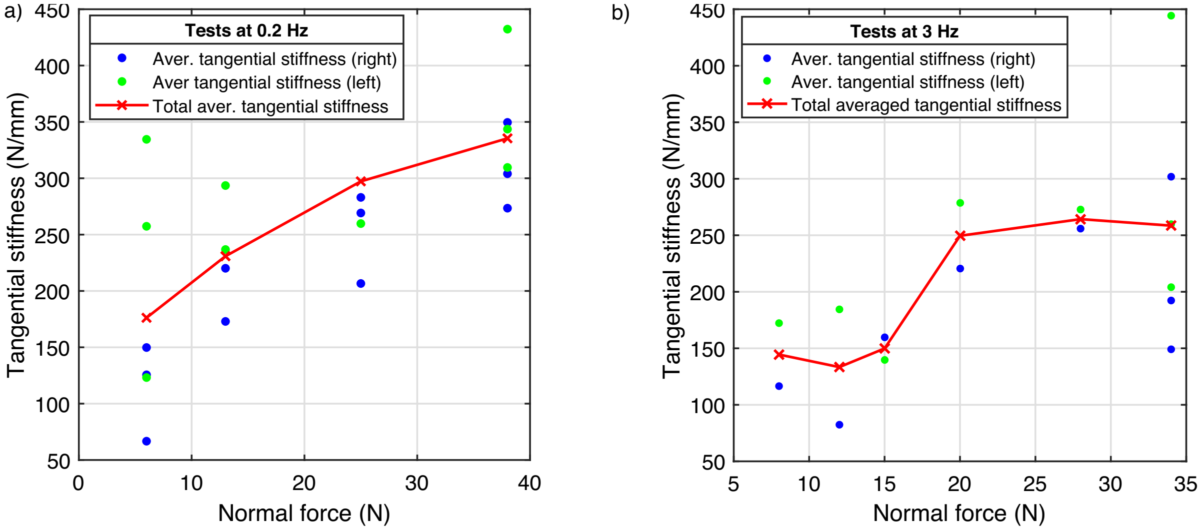

Fig. 14 Averaged tangential stiffness per tests and correlation with the measured normal force: (**a**) reciprocating tests at 0.2 Hz; (**b**) reciprocating tests at 3 Hz

4.5 One-way ANOVA and principal component analysis (PCA)

All data set were quantitatively assessed to check the statistical similarity or dissimilarity by means of a one-way analysis of variance (ANOVA) [44]. On top of that, a principal component analysis [44] was performed to establish the number of eventual independent factors that may drive the observed variance among the different tested specimens. The ANOVA test is a tool that enables the acceptance or rejection of the null hypothesis, which asserts that no relationship exists between two sets of data or that no difference between the groups exists. If the null hypothesis is true, any observation may be due to chance alone. In order to check the validity of the null hypothesis, the p-value probability is calculated, which estimates the likelihood of a sample occurring due to chance, given an assumed sampling distribution. If this probability is lower than a chosen threshold α, usually equal to 0.05, the null hypothesis can be rejected. In other words, a p-value lower than 0.05 means that the two groups are statistically different and the observed difference between the groups is not due to chance alone. It is important to note that a low p-value, computed between two data set, does not imply correlation, and that a high p-value does not necessarily mean that the null hypothesis is true. The latter case only suggests that there is not enough evidence to reject the null hypothesis (e.g. due to a high variance within groups).

In the previous subsection, it was shown that the estimated values of the tangential stiffness tend to vary according to a variation in the normal force, while the identified coefficient of sliding friction seems to be more sensitive towards other (uncontrolled) parameters, and no distinct trend of variation with reference to a change in the normal force was observed. Therefore, the ANOVA analysis was applied on the identified friction coefficients, to assess the statistical similarity. Figure 15 shows the estimated p-values for the tests performed at 0.2 Hz (Fig. 15a), and 3 Hz (Fig. 15b). The p-values are only estimated for different pairs of the specimens (off diagonal terms). For clarity, the numbering of the specimens 1-11 and 1-8, follows the same sequence of specimens shown in Fig. 13a and Fig. 13b. For Fig. 15a, the first three pairs (1-3) correspond to specimens tested under the same normal force. The same applies to the pairs formed between 4 to 6, 7 to 8 and 9 to 11. In general, there is no clear pattern regarding the distribution of the p-values. However, on one hand, it can be observed that most of the specimen pairs in Fig. 13b exhibit a low p-value, meaning that most of the subset of data are statistically different between each other (apart from few exceptions). This also applies to combinations that belong to the same cluster tested under the same normal force. On the

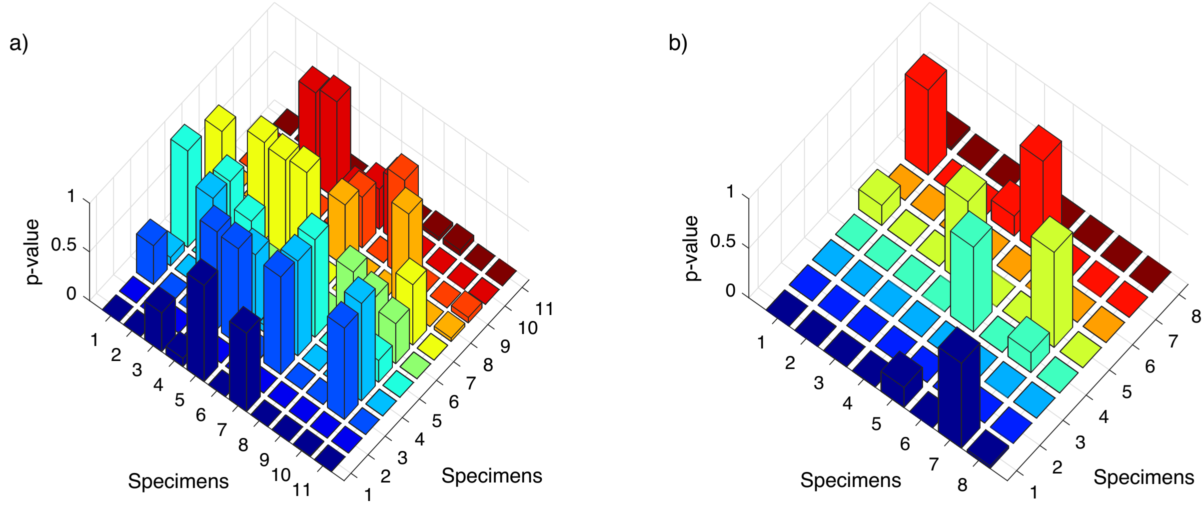

Fig. 15 One-way ANOVA applied in a pairwise way for the tests at 0.2 Hz (**a**), and 3 Hz (**b**). Note that the combinations along the main diagonal (e.g. 1-1, 2-2, etc.) are not evaluated

other hand, Fig 13a shows a more "equal" distribution between very low and high *p*-values, irrespective on whether or not the assessed combination belongs to the group tested under the same normal force. As a final note, specimen 2 (C2-3-38-A) and 11 (C2-4-6-A) seem to be statistically different from all other subsets of data. The pronounced statistical difference between the various data sets may be due to the different surface texture conditions of each specimen, since they resulted from a deliberate cracking process. The latter can be considered as an uncontrolled variable, introduced to mimic initial conditions present during shear couplet tests once the transition from cohesion loss to friction occurs.

Besides looking for hints for possible correlations between the data, a PCA was applied on both estimated quantities: coefficient of sliding friction and tangential stiffness. The PCA enables a linear mapping of the data from the original dimension n to a reduced dimension m, while retaining the most dominant patterns of the original data, which contribute mainly to its variance. For example, let a y_k, represent a standardised vector gathering the coefficients of sliding friction (or estimated tangential stiffness values), for every cycle N, for a specific specimen. Therefore, all the samples can be collected in a matrix $\mathbf{Y} \in \mathbb{R}^{nxN}$, in which n represents the different specimens. Hence, the linear mapping to a lower dimension m reads as follows

$$\mathbf{X} = \mathbf{TY} \tag{3}$$

in which $\mathbf{X} \in \mathbb{R}^{mxN}$ includes the Principal Component Scores (PCSs), and $\mathbf{T} \in \mathbb{R}^{mxn}$ is the loading matrix. The new dimension m can be seen as the number indicating the new physical order of the system, linked to the number of independent factors that can explain the main variance of the observed samples. To get the new dimension m, the Singular Value Decomposition (SVD) is applied on the covariance matrix of the estimated samples $\mathbf{YY}^T$, which gives

$$\mathbf{YY}^T = \mathbf{U\Sigma U}^T \tag{4}$$

where $\mathbf{U}$ define the Principal Components, the singular values are given by the diagonal terms of matrix σ. Such singular values quantify the active energy of the associated Principal Components. To define the m number of factors that can explain the largest part of the observed variance, the cumulative sum of singular values divided by the total sum of singular values is computed. As a rule of thumb, m is chosen as the smallest number of singular values able to capture the 70–90% of the total variance. Note that the factor analysis does not indicate a physical link between factors and physical parameters, it only provides (in a linear regression framework), the minimum number of factors that may be able to explain the observed variation.

The PCA is carried out on both the estimated coefficients of sliding friction and the tangential stiffness values. The analysis is performed by inspecting the data set in two different ways. For the analysis 1, the PCA aims to detect the minimum number of independent factors that explain the variance over the different reciprocating sliding cycles, whereas analysis 2 aims at detecting the minimum number of factors that explain the variance across different material pairs (i.e. across the variation of the normal force), for every cycle. The latter can be achieved by transposing the original matrix **Y**.

Figure 16a relates to analysis 1, in the attempt to identify common patterns throughout the cycles. A 70% to 90% of variation, for both the tangential stiffness and the estimated coefficients of sliding friction, can be captured by two to four independent factors. This seems to be valid regardless of the tested frequency. For analysis 2, which attempts to identify common patterns among the various specimens, for the different cycles, one factor seems to already capture 70% of the variation for the tangential stiffness (independently of the frequency), whereas two factors can explain the 90% of the observed variation. According to Fig. 14, the first factor could well be the normal force, which is the varying parameter between the different tested specimens. The second factor could be linked to the wear or degradation process which seems to exhibit a common trend across the different specimens as shown in Fig. 11a. With reference to the estimated coefficient of sliding friction, two to four factors are needed to explain the 70% to 90% of variation, see Fig. 16a. In general, regardless the method of analysis, the factors defining the variation for the coefficients of sliding friction are rather hard to pin down, besides the obvious link towards the wear process which occurs throughout the cycles. It is important to emphasise that all the data are inclusive of the running-in phase, since the goal of this experimental work was to assess the variability of the coefficient of friction during the first cycles that occur at the mortar-brick interface after a crack has formed.

5 Discussion and conclusion

5.1 Limitations and future research directions

To understand the frictional response of cracked brick-mortar interfaces, a reciprocating tribometer testing procedure has been developed and a preliminary experimental test series has been carried out on clay brick masonry with cement-lime mortar. Differently than available testing procedure for masonry interface tests, such as triplet and couplet tests, this approach allows to isolate the frictional response

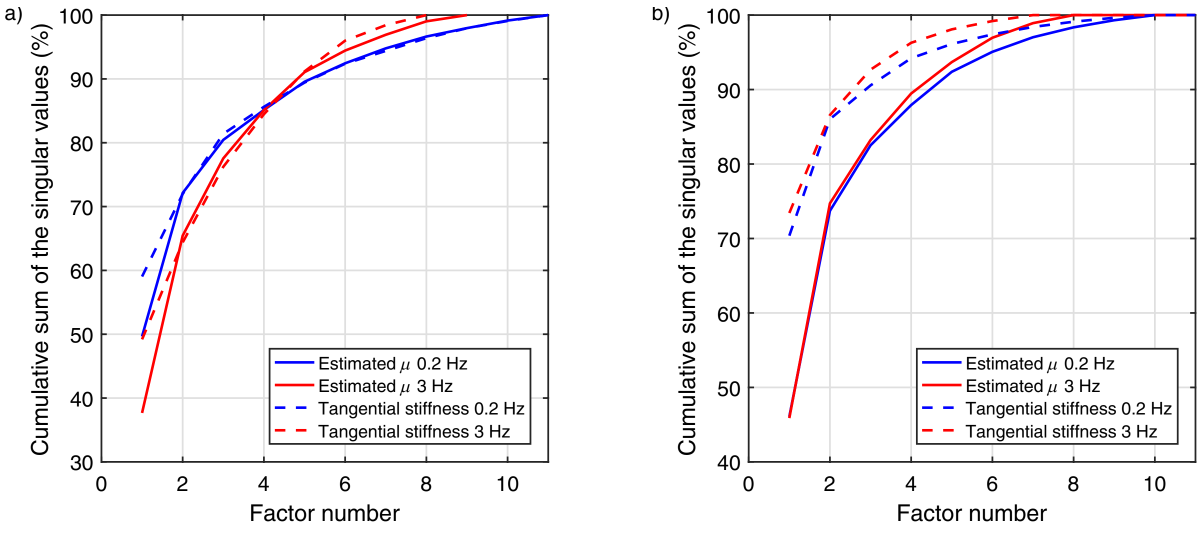

Fig. 16 Principal component analysis (PCA): (**a**) method of analysis 1, to inspect the number of factors explaining the variance across cycles; (**b**) method of analysis 2, to inspect the number of factors explaining the variance across material pairs. The PCA is applied to the identified coefficient of sliding friction and tangential stiffness, at 0.2 Hz and 3 Hz

from the one related to de-cohesion mechanism. This research also represents an initial attempt to assess the variability of tribological parameters – specifically, the coefficients of sliding friction and tangential stiffness – during the running-in phase of a mortar-brick interface. Results indicated significant variability (because estimated during a running-in phase), although the measured coefficients of sliding friction aligned well with values estimated through traditional methods typically used to assess the shear properties of masonry couplets or triplets.

One of the key limitations of this study was the uncontrolled initial surface conditions. These conditions were deliberately determined by the fracture process that occurred before the friction tests, rather than being intentionally prepared. This lack of control contributed to:

- A lack of symmetry in the hysteresis curves, complicating the interpretation of the results, particularly regarding the tangential stiffness.
- Significant variability in the initial conditions across tested specimens, which also led to low *p*-values (see ANOVA results in Fig. 15) for data sets tested under the same normal load.

Based on the findings and challenges encountered, several recommendations are proposed to improve future testing campaigns:

(a) Reduced initial loading rate at the onset of reciprocating sliding (first pull), to better capture the transition from static to kinetic friction.
(b) Varying loading rates during the first pull, to investigate any dependency between loading rate, initial tangential stiffness, and the static-to-kinetic friction transition.
(c) Monitor the wear and degradation process more closely. Reciprocating sliding tests should be accompanied by continuous surface scanning–before, during (if possible), and after testing, to analyse the influence of wear and debris on the frictional behaviour of the mortar-brick interface.
(d) Conduct tests on surfaces with varying and controlled initial roughness levels to assess their influence on friction behaviour.
(e) Due to the large scatter observed in the data, a significantly larger sample size is recommended for future test series to characterise a single masonry typology under each specific loading condition.
(f) In order to minimise the material variability for a given specimen (material pair), it could be recommended to prolong the number of cycles during a test, and seek for a “steady-state” regime, during which the hysteresis cycles are less scattered. However, reaching a possible steady state may highly depend on the initial roughness conditions and the sensitivity to wear.

5.2 Conclusions

The kinetic coefficient of sliding friction was consistently identified within the range of 0.4 to 0.6, with no clear dependency on the applied normal load observed from the tests. Statistical analysis, specifically the one-way ANOVA, indicated significant differences among several data set combinations, as evidenced by *p*-values below 0.05 in most comparisons.

Dissipated energy was generally higher during the initial cycles, stabilising towards a plateau after approximately 50 cycles at 3 Hz. This trend seemed to occur also for the tests at 0.2 Hz. The tangential stiffness, governing the transition from static to kinetic friction, exhibited high variability, with median values ranging between 100 and 400 N/mm. A qualitative dependency of the tangential stiffness on normal load was also noted.

The factor analysis revealed that the variability in both tangential stiffness and the coefficient of friction appears to be influenced by two to four independent factors, when considering the variation over the cyclic repetitions. However, for tangential stiffness specifically, differences between tests at varying normal loads could be attributed to only one or two dominant factors, supporting the eventual dependency to the normal load.

It should be noted that the trends identified in this study refer only to one masonry typology. Additionally, considering the above-mentioned limitations, trends and dependencies should be considered as preliminary. Further experiments are thus required to identify what are the factors governing the friction behaviour.

Despite the limitations of the findings, this paper initiates a new methodology to evaluate the frictional response of cracked brick-mortar interface for traditional mortaredmasonry. By combining this test with more conventional shear-compression tests on sound brick-mortar interfaces (i.e., triplets and couplets tests), it will be possible to evaluate what is the contribution of de-cohesion and friction mechanisms in shear failure of masonry interfaces. Besides being relevant for laboratory tests, the approach could also be considered for the characterisation of existing masonry constructions due to the limited size of the specimens that may need to be extracted.

Author Contributions Rita Esposito: Conceptualization, Methodology, Investigation, Resources, Writing–Original Draft, Writing–Review and Editing. Karthick Sasikumar: Investigation, Data Curation. Alessandro Cabboi: Conceptualization, Methodology, Investigation, Formal analysis, Visualization, Data Curation, Writing–Original Draft and Editing.

Funding This research did not receive any specific grant from funding agencies in the public, commercial, or nonprofit sectors.

Data Availability All data generated or analysed during this study are available from the authors upon reasonable request via email.

Declarations

Conflict of interest The authors have no conflict of interest to declare that are relevant to the content of this article.

Ethical Approval The authors state that the research was conducted according to ethical standards. This article does not contain any studies with human participants or animals performed by any of the authors.

References

1. Ferretti F, Ferracuti B, Mazzotti C, Savoia M (2019) Destructive and minor destructive tests on masonry buildings: experimental results and comparison between shear failure criteria. Constr Build Mater 199:12–29
2. Montazerolghaem M, Jaeger W (2014) A comparative numerical evaluation of masonry initial shear test methods and modifications proposed for EN 1052-3. In: Proceedings of the 9th International Masonry Conference
3. Riddington J, Jukes P (1994) A masonry joint shear strength test method. Proceedings of the Institution of Civil Engineers-Structures and Buildings 104(3):267–274
4. Pluijm R (1999) Out-of-plane bending of masonry: behaviour and strength. Phd thesis, Eindhoven Technical University https://pure.tue.nl/ws/files/1570536/528212.pdf
5. Segura J, Bernat E, Mendizábal V, Pelà L, Roca P, Gil L (2021) Experimental comparison of two testing setups for characterizing the shear mechanical properties of masonry. J Build Eng 44:103277
6. Riddington JR, Fong KH, Jukes P (1997) Numerical study of failure initiation in different joint shear tests. Masonry Int 11(2):44–50
7. Popal R, Lissel S (2010) Numerical evaluation of existing mortar joint shear tests and a new test method. In: Proc. 8th International Masonry Conference, Dresden
8. Barattucci S, Sarhosis V, Bruno AW, D'Altri AM, de Miranda S, Castellazzi G (2020) An experimental and numerical study on masonry triplets subjected to monotonic and cyclic shear loadings. Constr Build Mater 254:119313
9. Ferretti F, Mazzotti C, Esposito R, Rots JG (2018) Shear-sliding behavior of masonry: numerical micro-modeling of triplet tests. In: Computational Modelling of Concrete Structures, pp. 941–951. CRC Press, Leiden, The Netherlands
10. CEN: EN-1052-3 Methods of test for masonry - Part 3: Determination of initial shear strength (2002)
11. Rios AJ, Nela B, Pingaro M, Reccia E, Trovalusci P (2025) Parametric analysis of masonry arches following a limit analysis approach: Influence of joint friction, pier texture, and arch shallowness. Math Mech Solids 30(1):137–165
12. Rios AJ, Pingaro M, Reccia E, Trovalusci P (2022) Statistical assessment of in-plane masonry panels using limit analysis with sliding mechanism. J Eng Mech 148(2):04021158
13. Casapulla C, Argiento L (2016) The comparative role of friction in local out-of-plane mechanisms of masonry buildings. pushover analysis and experimental investigation. Engineering Structures 126, 158–173
14. Vlachakis G, Colombo C, Giouvanidis AI, Savalle N, Lourenço PB (2023) Experimental characterisation of dry-joint masonry structures: Interface stiffness and interface damping. Constr Build Mater 392:130880
15. Savalle N, Lourenço PB, Milani G (2022) Joint stiffness influence on the first-order seismic capacity of dry-joint masonry structures: Numerical dem investigations. Applied Sciences **12**(4)
16. Jafari S, Rots JG, Esposito R (2020) Core testing method to assess nonlinear shear-sliding behaviour of brick-mortar interfaces: A comparative experimental study. Constr Build Mater 244:118236
17. Jafari S (2021) Material characterisation of existing masonry: A strategy to determine strength, stiffness and

toughness properties for structural analysis. Phd thesis, Delft University of Technology https://doi.org/10.4233/uuid:3bcbbc72-0212-44e9-ac86-2fdc54ec5987

18. Gaggero MB, Esposito R (2023) Experimental characterisation of flexural bond behaviour in brick masonry. Mater Struct 56(3):62
19. Graziotti F, Tomassetti U, Kallioras S, Penna A, Magenes G (2017) Shaking table test on a full scale URM cavity wall building. Bull Earthq Eng 15:5329–5364
20. Zmitrowicz A (2005) Wear debris: a review of properties and constitutive models. Journal of Theoretical and Applied Mechanics **43**(1)
21. Godet M (1984) The third-body approach: A mechanical view of wear. Wear 100(1):437–452
22. Diomidis N, Mischler S (2011) Third body effects on friction and wear during fretting of steel contacts. Tribol Int 44(11):1452–1460
23. Mulvihill DM, Kartal ME, Olver AV, Nowell D, Hills DA (2011) Investigation of non-coulomb friction behaviour in reciprocating sliding. Wear 271(5):802–816
24. Hintikka J, Lehtovaara A, Mäntylä A (2016) Normal displacements in non-coulomb friction conditions during fretting. Tribol Int 94:633–639
25. Zheng Y, Cabboi A, Kuilen J-W (2024) Identification of the coefficient of sliding friction from an apparent non-Coulomb behavior between wood and steel. Tribol Int 200:110193
26. Fouvry S, Kapsa P, Vincent L (1995) Analysis of sliding behaviour for fretting loadings: determination of transition criteria. Wear 185(1):35–46
27. Argatov II, Chai YS (2023) A theoretical justification of the slip index concept in fretting analysis. Friction 11(7):1265–1275
28. Zanoria ES, Danyluk S, McNallan MJ (1995) Formation of cylindrical sliding-wear debris on silicon in humid conditions and elevated temperatures. Tribol Trans 38(3):721–727
29. Miftakhova A, Chen Y-Y, Horng J-H (2019) Effect of rolling on the friction coefficient in three-body contact. Adv Mech Eng 11(8):1687814019872303
30. Ghosh A, Wang W, Sadeghi F (2016) An elastic–plastic investigation of third body effects on fretting contact in partial slip. Int J Solids Struct 81:95–109
31. Chen X, Madden ASE, Reches Z (2017) Powder rolling as a mechanism of dynamic fault weakening. Geophys Monogr Ser 227:133–150
32. Costa HL, Oliveira Junior MM, de Mello JDB (2017) Effect of debris size on the reciprocating sliding wear of aluminium. Wear 376-377, 1399–1410
33. Oktay ST, Suh NP (1992) Wear debris formation and agglomeration. J Tribol 114(2):379–393
34. Zhang J, Moslehy FA, Rice SL (1991) A model for friction in quasi-steady-state sliding part I: Derivation. Wear 149(1–2):1–12
35. Zhang J, Mosleby FA, Rice SL (1991) A model for friction in quasi-steady-state sliding part II: Numerical results and discussion. Wear 149(1):13–25
36. Sherrington I, Hayhurst P (2001) Simultaneous observation of the evolution of debris density and friction coefficient in dry sliding steel contacts. Wear 249(3):182–187
37. Viáfara CC, Sinatora A (2011) Unlubricated sliding friction and wear of steels: An evaluation of the mechanism responsible for the T1 wear regime transition. Wear 271(9):1689–1700
38. Kumar R, Prakash B, Sethuramiah A (2002) A systematic methodology to characterise the running-in and steady-state wear processes. Wear 252(5):445–453
39. Ghiassi B, Vermelfoort A, Lourenço PB (2019) Masonry mechanical properties. In: Numerical Modeling of Masonry and Historical Structures, pp. 239–261
40. Atkinson R, Amadei B, Saeb S, Sture S (1989) Response of masonry bed joints in direct shear. J Struct Eng 115(9):2276–2296
41. Johnson KL (1985) Contact Mechanics. Cambridge University Press, Cambridge
42. Lourenço PB, Rots JG (1997) Multisurface interface model for analysis of masonry structures. J Eng Mech 123(7):660–668
43. Abdulla KF, Cunningham LS, Gillie M (2017) Simulating masonry wall behaviour using a simplified micro-model approach. Eng Struct 151:349–365
44. Johnson RA, Wichern DW (eds) (2002) Applied Multivariate Statistical Analysis. Prentice hall, Upper Saddle River, New Jersey, USA